

Fabrication and Mechanical Performance of a Mesoscale Space-Filling Truss System

Scott T. Brittain, Yuki Sugimura, Olivier J. A. Schueller, Anthony G. Evans, and George M. Whitesides, *Member, IEEE*

Abstract—A small, lightweight, space-filling truss structure is fabricated using soft lithography in combination with electrodeposition. The truss architecture is chosen so that three-dimensionality can be achieved simply by folding a two-dimensional grid at a specific angle. The mechanical performance and structural efficiency of the truss beam are assessed under four-point bending and compared to the bending behavior of a square box beam in terms of nondimensional indexes for stiffness, weight, and load-bearing capacity. [531]

Index Terms—Design optimization, electrodeposition, mesoscale trusses, performance indexes, soft lithography.

I. INTRODUCTION

THIS paper describes a method for the fabrication of a metallic space-filling truss in which the structural elements have lengths on the order of millimeters and diameters of $\sim 200\ \mu\text{m}$. A truss is a rigid, lightweight, structural framework that defines a maximal amount of space with a minimal amount of material [1]–[3]. Trusses take advantage of the inherent stability of triangles: the angles of a triangle cannot change without changing the lengths of the sides [1]. This property imparts a high strength-to-weight ratio, since large spans can comprise relatively slender, widely spaced elements. For this reason, building designers commonly employ two-dimensional (2-D) truss systems as roof supports [Fig. 1(a)]. Whereas 2-D trusses utilize the triangle as the stabilizing unit, three-dimensional (3-D) trussed space frames utilize the tetrahedron [Fig. 1(b)] [3]. As with the 2-D case, 3-D space frames combine high strength with low weight and structural “openness.” Designers use these systems when it is necessary to span a large area, such as the ceiling of a gymnasium or natatorium. Related 3-D truss systems can form columns, beams, and nonplanar surfaces, including cylindrical vaults, and hemispherical domes [2].

The strategy used to produce steel trusses at the size scale of building materials, assembly of a large number of individually machined components using nuts, bolts, and welding, is not suitable for use at the submillimeter scale. Moreover, the industrial processes used to produce the steel components them-

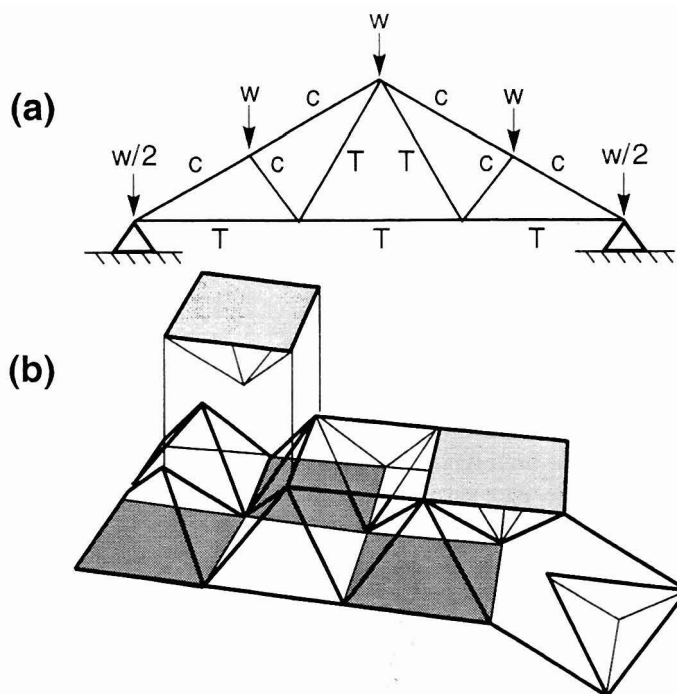


Fig. 1. (a) Weight (W) distributed over the top of a planar truss is apportioned among its members as tensile (T) and compressive (C) forces [1]. (b) A space-filling truss derives strength from the tetrahedral arrangement of its members. The truss system discussed in this paper can be more easily visualized as an interlocking array of square-based pyramids (shading added for visualization only.)

selves, rolling, casting, and forging, are not feasible at the meso- and microscale. It has been proposed [4]–[6] that electrochemical deposition and dissolution of metals will play a key role in the fabrication and assembly of metallic components at these small size scales. Microfabrication techniques such as LIGA (Lithographie, Galvano, and Abformung or lithography, electrodeposition, and molding) [7], [8] have grown out of the microelectronics industry. Using this and similar techniques, the fabrication of planar metallic structures has become routine. Aside from producing structures with high aspect ratios, however, these methods have not made much progress into the third dimension. Full three-dimensionality must be introduced either through layer by layer addition or by using serial techniques that carve microstructures from solid objects by laser micromachining [9], [10] or “write” 3-D microstructures [11], [12].

Here we present a new method for the fabrication of a 3-D trussed space frame in metal at the mesoscopic scale. Our technique provides a route to truly 3-D objects. It is from this three-dimensionality that our structures derive their strength. We convert simple 2-D patterns into complex 3-D objects. We

Manuscript received February 9, 2000; revised October 5, 2000. Subject Editor, H. Fujita.

S. T. Brittain and G. M. Whitesides are with the Department of Chemistry and Chemical Biology, Harvard University, Cambridge, MA 02138 USA.

O. J. A. Schueller was with the Department of Chemistry and Chemical Biology, Harvard University, Cambridge, MA 02138 USA. He is now with Surface Logix, Brighton, MA 02135 USA.

Y. Sugimura is with the Division of Engineering and Applied Sciences, Harvard University, Cambridge, MA 02138 USA.

A. G. Evans is with the Princeton Materials Institute, Princeton University, Princeton, NJ 08540 USA.

Publisher Item Identifier S 1057-7157(01)01594-3.

then interconnect and strengthen these objects using microelectrochemistry. The present method uses soft lithography [13], [14]—particularly microcontact printing [15]–[17]—to define 2-D patterns in a silver (Ag) film having feature sizes $\sim 100\ \mu\text{m}$ wide over a large area ($\sim 6\ \text{cm}^2$). Microelectrochemistry using a malleable metal (Ag) strengthens the patterned metal [18]–[20], and subsequent manipulation transforms these 2-D patterns into 3-D mesostructures. Electrochemical welding joins several levels by forming multiple connections in a single electrodeposition step.

The mechanical response of the mesoscale truss structure is evaluated in four-point bending. The structural performance and efficiency of the truss system is compared to those of a square box beam of comparable size and weight using nondimensional indexes that factor out the effects of material properties and the beam lengths.

II. FABRICATION

Our method uses rapid prototyping [21] and microcontact printing, μCP (Fig. 2), in combination with microelectrochemistry to form the initial 2-D grid patterns that make up the truss. Rapid prototyping describes the method we use to generate flexible, inexpensive photomasks having feature sizes as small as $20\ \mu\text{m}$. A design generated using a suitable computer-aided drawing (CAD) software application (Macromedia Freehand 7.0) is printed onto a transparency using a commercial laser-assisted image-setting system.¹ The transparency is used as a photomask to generate a relief pattern in a layer of photoresist. We produce an elastomeric “stamp” by molding this relief pattern into polydimethyl siloxane.² The stamp, which carries the inverted relief pattern on one face, transfers a monomolecular pattern of a chemical “ink” to a substrate. In this study, the substrate consisted of glass microscope slide coated with Ti (5 nm, adhesion promoter) and Ag (50 nm) using an e-beam evaporator. The ink was a 1-mM solution of hexadecanethiol ($\text{CH}_3(\text{CH}_2)_{15}\text{SH}$, “HDT”). HDT forms a self-assembled monolayer (SAM) on the surface of Ag that acts as a nanometer-thick resist to subsequent wet chemical etching. Immersion of the substrate in an aqueous ferricyanide solution (0.001 M $\text{K}_4\text{Fe}(\text{CN})_6$, 0.01 M $\text{K}_3\text{Fe}(\text{CB})_6$, and 0.1 M $\text{Na}_2\text{S}_2\text{O}_3$) for 20–30 s removed the underivatized areas of Ag; immersion in aqueous HF (1%) for 15–20 s removed the areas of Ti exposed by the ferricyanide etchant. The result was a supported pattern in Ag that duplicated the pattern in the PDMS stamp. After electrically contacting the Ag pattern, we immersed the glass substrate in an Ag electroplating bath³ at room temperature and electrodeposited Ag at a current density of $\sim 20\ \text{mA}/\text{cm}^2$ for 15 min. At this point, the adhesion between the electroplated Ag layer and the initial vapor-deposited layer was sufficiently poor to make possible manual separation of the Ag grid structure from the substrate using tweezers.

As described in [1], the 3-D truss can also be assembled from its component set of grids, two of which are planar and one non-planar (Fig. 3). The latter, labeled B, defines the edges of the

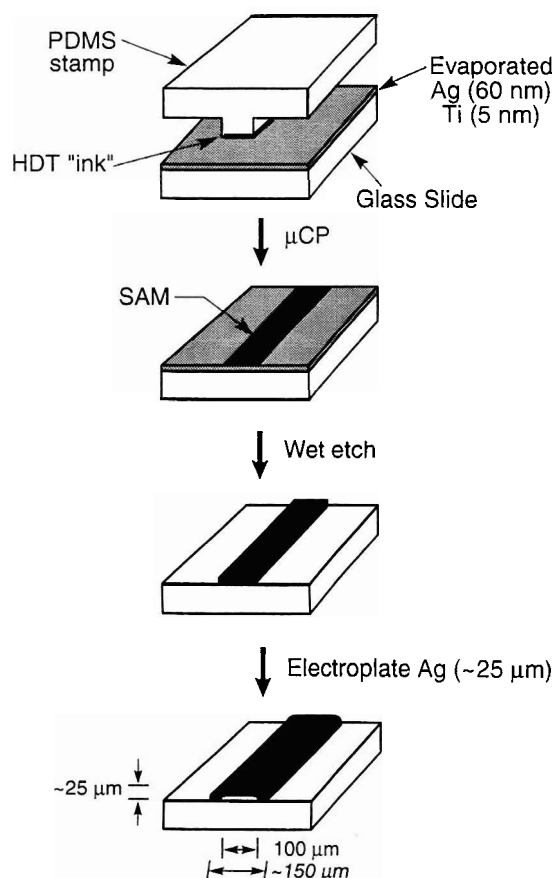


Fig. 2. Outline of the fabrication method consisting of μCP and electrodeposition. Elevated areas of a PDMS stamp transfers an HDT “ink” to the Ag surface. The SAM that forms in areas contacted by the stamp resists wet chemical etching of the underlying Ag in aqueous ferricyanide solution. Immersion of the substrate in HF solution removes the exposed Ti adhesion layer. Electroplating increases the thickness of the patterned Ag and enhances the overall strength for subsequent electrodeposition.

triangular sides of the square-based pyramids in the array. The top and bottom square grids make up the bases of the inverted and upright pyramids, respectively, in the array. These were prepared by μCP and electroplating, as described above. The diagonals supporting the square grids add lateral stability to the structure by converting each square into two triangles. The 3-D grid B can be unfolded along the indicated axes to produce the 2-D grid labeled A. To make B, we first fabricated A using μCP on a planar substrate, followed by electroplating; we then folded the sheet along the indicated axes using tweezers. Stamping of the folded grid with a machined brass die ensured that the folds achieved the desired 70° angle.

We aligned the three grids manually, as shown in Fig. 3, by using a stereomicroscope to aid visualization. The grid sections measured $\sim 1\ \text{cm} \times 2\ \text{cm}$, and each square cell measured $\sim 2\ \text{mm} \times 2\ \text{mm}$. Application of silver paint to the outer corners of the grids (indicated by dashed lines) affixed the grid temporarily for the electroplating step. An Sn wire electrically contacted the structure. We sandwiched the truss between sections of glass microscope slides and placed the assembly in a shallow Ni electroplating bath⁴ held at 45°C . A 50-g weight placed onto the glass slide ensured close contact between the grids during

¹Hercules PRO, 3387 dpi, Linotype-Hell Company, Hauppauge, NY.

²PDMS, Sylgard 184, Dow Corning, Midland, MI.

³Techni-Silver E2, Technic Inc., Providence, RI.

⁴Techni-Nickel-S, Technic Inc., Providence, RI.

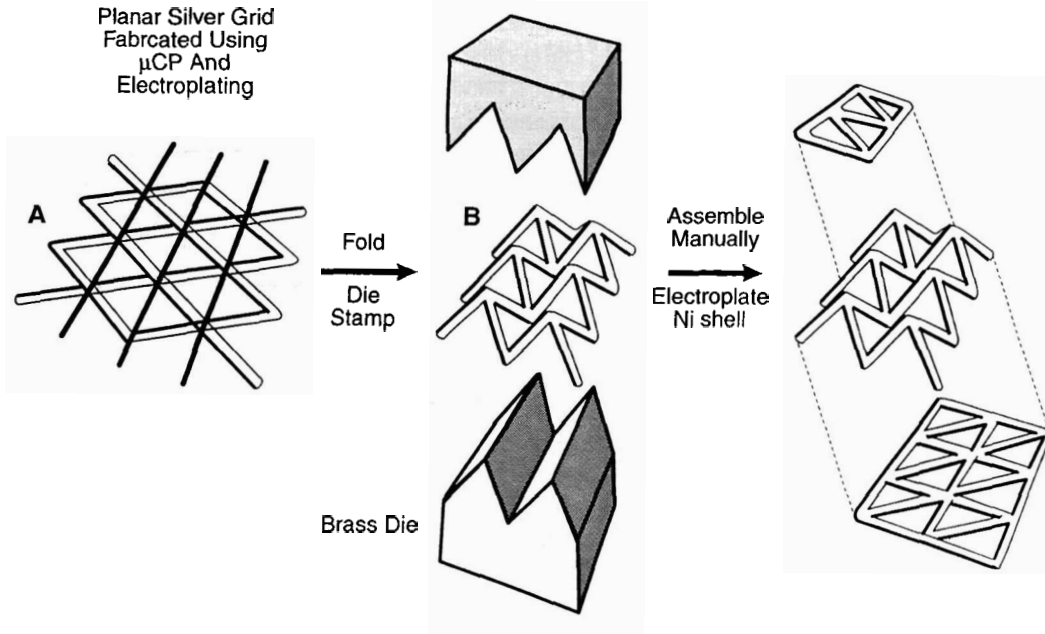


Fig. 3. Schematic depicting the fabrication of the 3-D truss system. A planar silver grid (labeled A) produced by μ CP and electroplating is manually folded with a brass die along the orientation indicated in the figure. The resulting 3-D structure is shown as B. The members of grid B comprise the edges and apexes of the triangular faces of the square-based pyramids in the array [refer to Fig. 1(b)]. The upper and lower grids are aligned with grid B as indicated by the dashed lines, and the corners are affixed with silver paint. Electrodeposition of Ni on the Ag template joins the three layers of grids and strengthens the overall 3-D truss system.

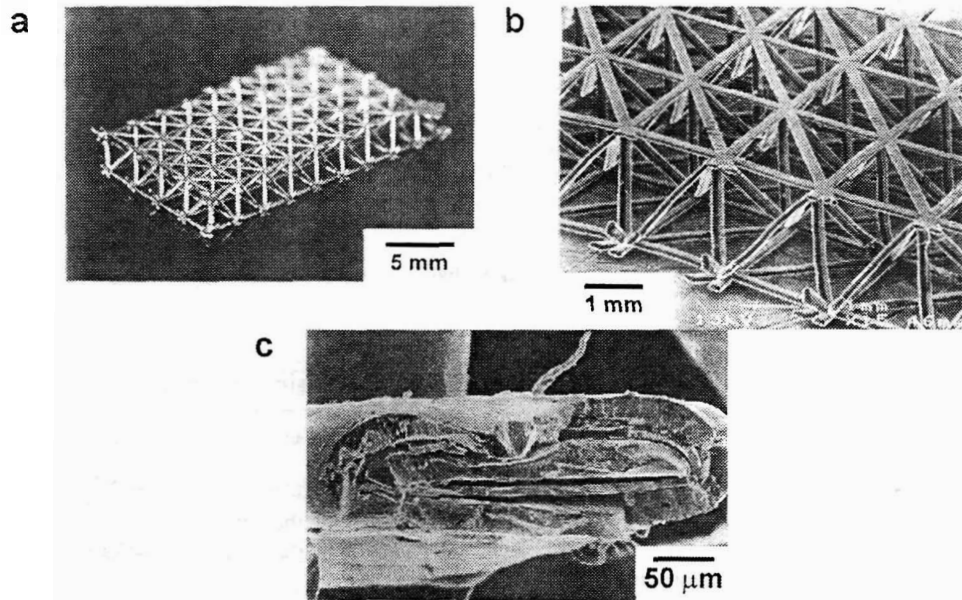


Fig. 4. (a) Photomicrograph showing a microtruss fabricated by assembling three Ag grids: two planar and one folded. Subsequent electrodeposition of a structural metal (Ni) over the malleable template (Ag) encapsulated, strengthened, and joined the three grids. (b) SEM image showing several of the electrowelded joints. (c) Strut cross section revealing the Ag core and the Ni shell.

electroplating. After electroplating at a current density of ~ 20 mA/cm² for 1 h, we removed the weight and the glass slides and electroplated at this current density for an additional 30 min to allow deposition on the top and bottom faces of the truss. Fig. 4(a) and (b) shows the completed truss.

III. BOX BEAMS

Beams subject to bending are commonly stiffened using I-s, boxes, and tubes. The minimum weights depend on the configuration, loading, and potential failure modes. Comparisons are facilitated by adopting nondimensional indexes [22].

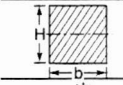
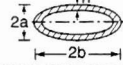
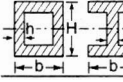
These indexes allow explicit effects of material properties and beam lengths to be factored out. Such indexes are used for the bending moment to be supported without failure, designated Π ; the weight ψ ; and the relative bending stiffness, or shape factor, ϕ . For beams subject to pure bending (no shear forces), these indexes are given by [22]

$$\Pi = M/L^3 \sigma_Y \quad (1a)$$

$$\psi = W/\rho_s L^3 \quad (1b)$$

$$\phi = S/S_0 \quad (1c)$$

TABLE I
SHAPE FACTOR FOR COMMON CROSS SECTIONS

	ϕ
	$\frac{\pi}{3} \left(\frac{H}{b} \right)$
	$\left[\frac{a}{h} \right] \frac{(1+3b/a)}{(1+b/a)^2}$
	$\frac{\pi}{6} \left[\frac{H}{h} \right] \frac{(1+3b/H)}{(1+b/H)^2}$

where

- M bending moment on the beam;
- L its length;
- W its weight;
- σ_Y yield strength;
- ρ_s density of the material;
- S stiffness of a shaped beam with cross-sectional area A ;
- S_o that for a solid beam having a circular cross section and the same cross-sectional area A .

Shape factors for some simple sections are summarized on Table I. The stiffness scales with the second moment of area I

$$S = B_1 EI / L^3 \quad (2a)$$

where E is Young's modulus and B_1 is a constant that depends only on the loading details (Table II). Accordingly, the only measure of stiffness associated with shape is the second moment of area I , enabling the shape factor to be reexpressed as

$$\phi \equiv I / I_o \quad (2b)$$

where I_o refers to the solid circular section

$$I_o = A^2 / 4\pi. \quad (2c)$$

Another useful expression for the shape factor obtained from (2b) and (2c) is thus

$$\phi = 4\pi I / A^2. \quad (2d)$$

With reference to Table I and from (2d), it is apparent that for a box beam with fixed A (i.e., constant weight), the shape factor can be increased without limit by allowing the wall thickness to approach zero. In practice, there are limits because of failure modes that arise as ϕ becomes large. Consideration of all potential failure modes is a crucial aspect of weight optimization. Yielding, overall, and local buckling are the three major possibilities.

When these failure modes are included in the design, there is a maximum realizable shape factor. The maxima used in practice may be found by measuring the second moment of area I , as well as the area of the cross section A of commercially used beams and cross plotting on logarithmic axes. Results for steel beams are summarized on Fig. 5. Lines of slope 2 [see (2d)] represent constant shape factors. It is apparent from the figure that the shape factor for box beams has a maximum, $\phi_{\max} \approx 20$, while that for I-beams is $\phi_{\max} \approx 65$. Hereafter, box beams are

emphasized since they are similarly effective in bending and torsion (I-beams are only useful in bending) [22]. To gain some understanding of these maxima, the failure modes can be represented on a map that comprises a cross plot of the load index Π against the shape factor ϕ . One such map, determined for box beams, is presented in Fig. 6, wherein the location of the domain boundaries depends on the yield strain for the material ϵ_Y . Fig. 6 refers to a yield behavior typical of that for pure metals ($\epsilon_Y \approx 7.5 \times 10^{-4}$). The figure should be interpreted as follows. Configurations and loads that reside in the buckling domain must be avoided; otherwise, the beams would fail catastrophically. This requirement limits ϕ to be less than 36: conservatism leads to the lower values $\phi \leq 20$ used in practice (see Fig. 5). The maximum values of the load index Π are governed by the avoidance of plastic failure. A conservative design would assure that the response of the beam is entirely elastic. However, since the limit loads appreciably exceed those at yield, designing beyond yield is permissible in some cases. Accordingly, the maximum allowable load index consistent with the maximum practical shape factor is $\Pi_{\max} \approx 10^{-5}$. The practicable stiffness consistent with the maximum realizable loads is plotted as the cross-hatched area in Fig. 6, which can be used to compare box beams with competing configurations. The interplay between stiffness, load capacity, and weight can now be addressed. For this purpose, note from Table I that for a stiff square box beam (wall thickness h much less than the beam height H)

$$\phi = (\pi/6)(H/h) \quad (3a)$$

and

$$W = 4hHL\rho_s \quad (3b)$$

such that the weight index from (1b) is

$$\psi = (4\pi/6)(H/L)^2 \phi^{-1}. \quad (3c)$$

Consequently, at maximum stiffness ($\phi = 20$), the weight is

$$\psi \approx (\pi/30)(H/L)^2. \quad (3d)$$

Note that if the external dimensions (H and L) are fixed, in general by thinning the wall (smaller h), the stiffness may be increased as well as the weight reduced but at diminished load capacity (Fig. 6).

IV. TRUSS BEAMS

A. Rationale

In order to explore the structural attributes of the space-filling truss, relative to the box beam, we fabricated a 3-D truss comprising a single row of pyramidal cells [Fig. 7(a)]. There are no theoretical results for such beams. The approach taken here is to make measurements in bending and to represent the results in a format that allows them to be compared directly with box beams. The measurements use the four-point bending procedure (see Fig. 8). In the regions between the outer and the inner load points ($0 \leq x \leq a$) and ($L-a \leq x \leq L$), the beam experiences a constant shear force and a linearly varying bending moment. Between the inner load points ($a \leq x \leq L-a$), there is a constant bending moment and no shear. The flexural rigidity EI

TABLE II
COEFFICIENTS FOR Laterally Loaded Beams

Loading		B ₁	B ₂	B ₃	B ₄
Cantilever	End	3	1	1	1
	Uniform	8	2	2	1
Both ends simply supported	Central	48	4	4	2
	Uniform	384/5	8	9	2
Both ends clamped	Central	192	4	9	2
	Uniform	384	8	12	2

*B₃ and B₄ respectively relate the bending moment, M , and the shear, Q , to the applied load, P , such that $M = PL/B_3$ and $Q = P/B_4$.

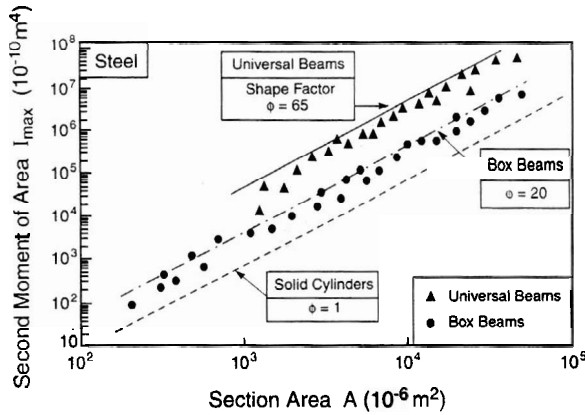


Fig. 5. A cross plot of the moment of area I against the area of cross section A for steel box and universal beams used in practice for bending applications. The diagonal lines of slope 2 indicate the median values of the shape factor ϕ .

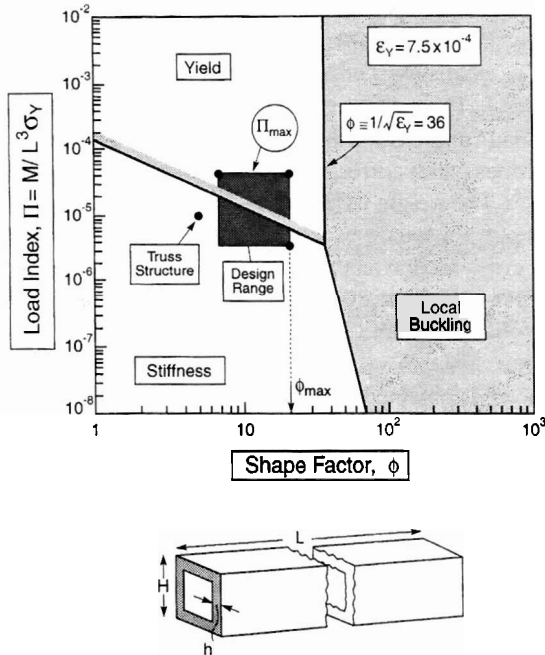


Fig. 6. A failure map for box beams showing domain boundaries and the conservative design range.

is obtained by measuring the difference between the load point displacement and the central (maximum) deflection as a func-

tion of load P . Then, since $S \equiv \delta/P$, the moment of area I can be obtained from (2a). Once EI has been measured in this manner, it is also possible to obtain the shear rigidity GA from the load point displacement, δ_P using

$$S_P \quad \delta_P/P = \frac{L^3}{B_1 EI} + \frac{L}{B_2 GA}. \quad (4)$$

Since the area of the cross section is

$$A = bH(\rho/\rho_s) \quad (5)$$

where

- ρ density of the geodesic beam;
- b beam width;
- H specimen height.

The effective shape factor is obtained from (2d), (4), and (5) as

$$\phi = \frac{4\pi SL^3}{B_1 E(bH)^2(\rho/\rho_s)^2}. \quad (6)$$

B. Measurements

The truss beams had dimensions $b = 3.3$ mm, $H = 2.0$ mm, strut diameter $d = 320$ μ m, and relative density $\rho/\rho_s \approx 0.12$. For four-point testing, the outer span $L = 31.75$ mm and inner span $2a = 15.88$ mm. The specimens were displaced at 20 μ m/s. The load-point displacement, as well as the central deflection, were recorded as a function of applied load. A typical load-displacement curve is shown in Fig. 8. The behavior is linear until a load drop is exhibited at about 30 N. The linear region gives the required stiffness information. There are subsequent load oscillations, accompanied by a general strain softening. After testing beyond the load drop, examination in the scanning electron microscope (SEM) revealed two predominant features: indentation of the strut members at the load pins [Fig. 7(d)] and fracture of some axial struts at the tensile extremity [Fig. 7(b) and (c)]. The latter are located in the constant moment region between the inner loading points. They occurred with minimal plastic distortion because the nanosized grains in as-deposited Ni cause it to behave in a brittle manner. Accordingly, the peak loads, on a relative basis (through Π), are lower than the full capacity of this beam design should the struts be composed of a ductile structural alloy. A cursory estimate of the actual load capacity has been found by annealing the truss

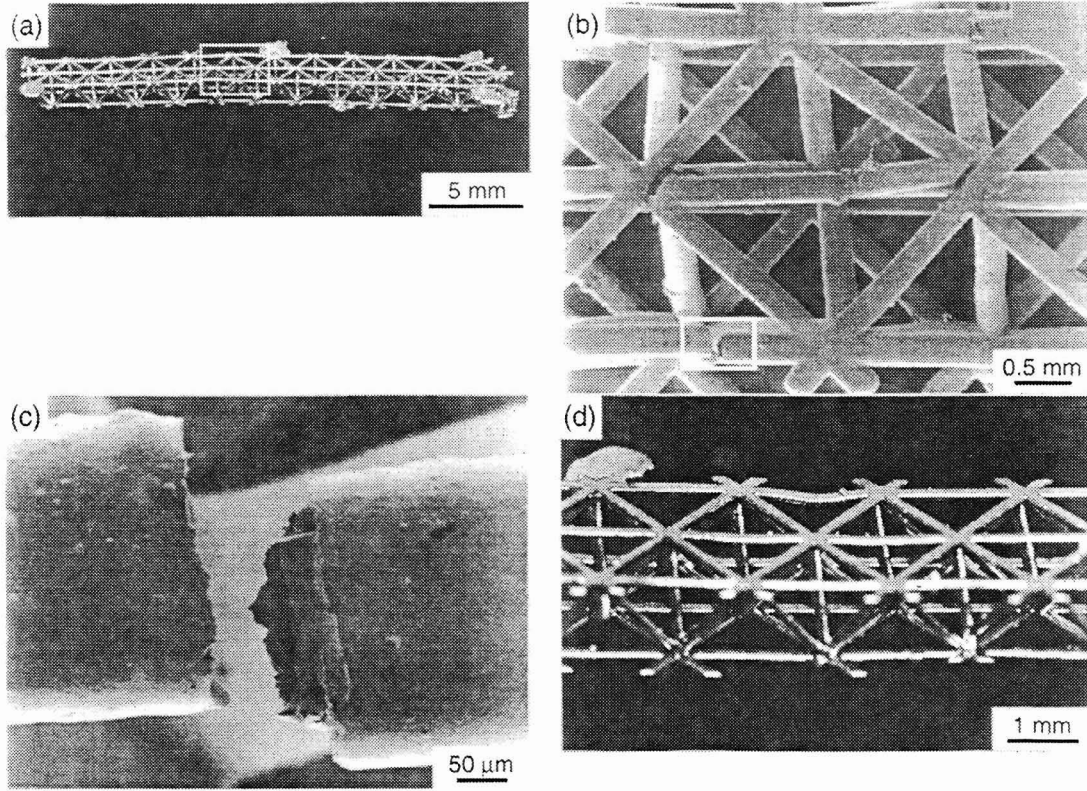


Fig. 7. Photomicrographs of truss beam after bend test showing (a) the entire specimen, (b) fractured struts and nodes in the area indicated by the rectangle in (a), (c) magnified view of fractured strut (note the lack of ductility in the as-deposited Ni and the core/shell morphology), and (d) indentation of the strut at the load point.

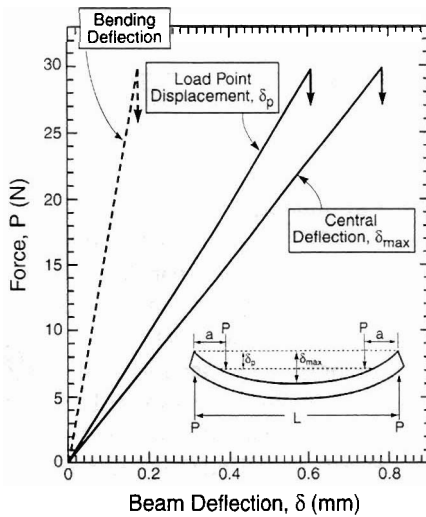


Fig. 8. Typical load-displacement curves for four-point bending of truss beam.

material in vacuum at 750 °C for 8 h to grow the grains and restore some ductility. Retesting after annealing revealed greater ductility, albeit somewhat compromised by porosity generated during annealing. Nevertheless, the response was nonlinear, and the peak loads provide some information relevant to the load index, discussed next. Microhardness measurements made on the truss members after annealing indicate a yield strength of $\sigma_Y \approx 60$ MPa (in the range expected for “pure” Ni).

V. PERFORMANCE INDEXES

Using the stiffness measured in the linear region (Fig. 8), EI and GA have been obtained from (2a) and (4) as 0.051 Nm² and 1400 N, respectively. The associated shape factor obtained from (6) is $\phi \approx 5$. The maximum moment sustained by the beam at the peak load (upon using the yield strength estimated from the microhardness test) corresponds to a maximum load index $\Pi_{\max} \approx 10^{-5}$. The weight index is 9×10^{-4} . The shape factor and load index for a square box beam having the same weight and external cross section as the truss are used for comparison. Such a beam would have 80- μ m-thick walls. The associated shape factor obtained from (3) and Table I is $\phi \approx 16$ (close to the maximum realizable value). The maximum load index for this shape factor is obtained from Fig. 6 as $\Pi_{\max} \approx 2 \times 10^{-5}$.

The present truss is thus much less stiff than an optimized box beam made from the same material and having the same weight (Fig. 6). Its maximum load capacity is also lower. This result highlights the generally inferior performance of nonoptimized geometries. The next step in the development of a competitive truss material would be to vary the aspect ratio of the trusses and the truss architecture to seek configurations that have greater stiffness and strength. This search should be guided by theoretical results [23].

VI. CONCLUSION

The method we describe here uses soft lithography in combination with electrochemical plating and welding to fabricate a

space-filling truss—a complex 3-D object. We generate an array of interconnected submillimeter elements using a simple parallel stamping process. At a production scale, a metal-punching technique might prove a useful substitute to produce the initial planar metal structures. For small-scale prototyping in the chemical laboratory, however, we believe our soft-lithographic process to be simple, rapid, and cost effective. At smaller feature sizes, we believe microcontact printing will prove to be the superior technique: feature sizes as small as 1 μm are routine using this technique [13].

This procedure provides a general approach to the fabrication of open 3-D structures, provided that the structures can be decomposed into assemblies of flat, folded, and/or curved sheets. In addition, by taking advantage of die stamping to fix the angles of the folded sheet, we have designed a procedure that lends itself easily to automation. The current radius of curvature ($\sim 50\ \mu\text{m}$) at the angles produced by the die stamping technique could be improved significantly by using higher tolerance techniques for the production of the die itself. We believe that with automation and optimization of the folding process, we could reduce the volume of these structures by a factor of 1000. Examples of potential applications that take advantage of the fabrication technique discussed in this paper include structural components (e.g., wings) in microair vehicles, small space vehicles and robots, and highly direction-agile mesoscopic antennas. At smaller dimensions, such structures would be useful as read/write arms in disk drives, and components in MEMS structures and biomedical devices for microsurgery.

The specific truss architecture chosen for this preliminary study is less structurally efficient than an optimized box beam in terms of stiffness-to-weight and load capacity. However, other truss architectures can be envisioned that are much more competitive [23]. They involve different truss angles and aspect ratios. Moreover, open trusses provide for functionalities beyond structural efficiency that could not be realized with closed box configurations. These designs will be explored in future studies.

REFERENCES

- [1] J. E. Ambrose, *Simplified Design of Steel Structures*, 7th ed. New York: Wiley, 1997.
- [2] T. T. Lan and Y. Zhilian, "Space structures for sports buildings," in *International Colloquium on Space Structures for Sports Buildings*. London, U.K., 1987.
- [3] J. E. Ambrose, *Design of Building Trusses*. New York: Wiley, 1997.
- [4] W. Menz, W. Backer, M. Harmening, and A. Michel, "The LIGA technique—A novel concept for microstructures and the combination with Si-technologies by injection molding," in *Proc. IEEE Micro Electro Mechanical Systems*, Nara, Japan, Jan. 30–Feb. 2 1991, p. 69.
- [5] M. Madou, *Fundamentals of Microfabrication*. Boca Raton, FL: CRC Press, 1997.
- [6] L. T. Romankiw, *Proc. 4th Int. Symp. Magnetic Materials, Processes, and Devices: Applications to Storage and Microelectromechanical Systems (MEMS)*, Chicago, IL, Oct. 9–12, 1995, pp. 397–403.
- [7] A. Abraham, H.-D. Bauer, W. Ehrfeld, M. Gerner, M. Lacher, H. Lehr, H. Lowe, A. Michel, A. Ruf, H. Schisfst, M. Schmidt, and L. Weber, "Achieving mass fabrication of micro-optical systems by combining deep X-ray lithography, electroforming, micromolding and embossing," *Proc. SPIE*, p. 48, Apr. 13–14, 1994.
- [8] W. Menz, "LIGA and related technologies for industrial application," *Sensors Actuators*, vol. A54, no. 1–3, pp. 785–789, 1996.
- [9] E. C. Harvey, P. T. Rumsby, M. C. Gower, and J. L. Remnant, "Microstructuring by excimer laser," in *Proc. SPIE*, vol. 2639, Austin, TX, Oct. 23–24, 1995, pp. 266–277.
- [10] G. Chryssolouris, *Laser Machining—Theory and Practice*. New York: Springer-Verlag, 1992.
- [11] J. D. Madden and I. W. Hunter, "Three-dimensional microfabrication by localized electrochemical deposition," *J. Microelectromech. Syst.*, vol. 5, pp. 24–32, Mar. 1996.
- [12] K. Ikuta, K. Hirowatari, and T. Ogata, "Three dimensional micro integrated fluid systems (MIFS) fabricated by stereo lithography," in *Proc. IEEE Micro Electro Mechanical Systems*, Oiso, Japan, Jan. 25–28, 1994, p. 1.
- [13] Y. Xia and G. M. Whitesides, "Soft lithography," *Angew. Chem. Int. Ed.*, vol. 37, no. 5, pp. 550–575, Mar. 1998.
- [14] ———, "Soft lithography," *Annu. Rev. Mater. Sci.*, vol. 28, pp. 153–184, 1998.
- [15] A. Kumar and G. Whitesides, "Features of gold having a micrometer to centimeter dimensions can be formed through a combination of stamping with an elastomeric stamp and an alkanethiol ink followed by chemical etching," *Appl. Phys. Lett.*, vol. 63, no. 14, pp. 2002–2004, Oct. 1993.
- [16] A. Kumar, H. A. Biebuyck, and G. M. Whitesides, "Patterning self-assembled monolayers: Applications in material science," *Langmuir*, vol. 10, no. 5, pp. 1498–1511, May 1994.
- [17] Y. Xia, E. Kim, and G. M. Whitesides, "Microcontact printing of alkanethiols on silver and its application in microfabrication," *J. Electrochem. Soc.*, vol. 143, no. 3, pp. 1970–1979, Mar. 1996.
- [18] R. J. Jackman, S. T. Brittain, and G. M. Whitesides, "Fabrication of three-dimensional microstructures by electrochemically welding structures formed by microcontact printing on planar and curved substrates," *J. Microelectromech. Syst.*, vol. 7, pp. 261–266, June 1998.
- [19] R. J. Jackman, S. T. Brittain, A. Adams, M. G. Prentiss, and G. M. Whitesides, "Design and fabrication of topologically complex, three-dimensional microstructures," *Science*, vol. 280, no. 5372, pp. 2089–2091, June 1998.
- [20] R. J. Jackman, S. T. Brittain, A. Adams, H. Wu, M. G. Prentiss, S. Whitesides, and G. M. Whitesides, "Three-dimensional metallic microstructures fabricated using soft lithography and microelectrodeposition," *Langmuir*, vol. 15, no. 3, pp. 826–836, Feb. 1999.
- [21] D. Qin, Y. Xia, and G. M. Whitesides, "Rapid prototyping of complex structures with feature size larger than 20 μm ," *Adv. Mater.*, vol. 8, no. 1, pp. 917–919, Oct. 1996.
- [22] P. M. Weaver and M. F. Ashby, "Material limits for shape efficiency," *Progress Mater. Sci.*, vol. 41, no. 128, pp. 61–128, 1997.
- [23] N. Wicks and J. W. Hutchinson, "Optimal truss plates," *Int. J. Solids Struc.*, to be published.

Scott T. Brittain received the Ph.D. degree in chemistry from Harvard University, Cambridge, MA, in 2000.

He is currently an Assistant Professor of chemistry at Georgia College and State University, Milledgeville. His research interests include inexpensive prototyping methods for microfabrication. His teaching methods focus on bringing real-world technology into the undergraduate classroom.

Yuki Sugimura received the Ph.D. degree in materials science with minors in solid mechanics and geology from Brown University, Providence, RI, in 1994.

After teaching as an Adjunct Assistant Professor in the Department of Manufacturing Engineering, Boston University, in the spring semester of 1995, she became a Postdoctoral Fellow in the Division of Engineering and Applied Sciences, Harvard University, Cambridge, MA. She is currently a Research Associate at Harvard University, as well as an Instructor in the Orthopedic Research Laboratory at Brigham and Women's Hospital, Harvard Medical School. Her research interests include mechanics of materials, porous/lightweight multifunctional materials, thin films, and coatings used in industrial and biomedical applications.

Olivier J. A. Schueller received the Dipl.Ing. degree from the Ecole Supérieure de Chimie Organique et Minérale (ESCOM), Cergy-Pontoise, France, in 1991 and the Ph.D. degree in organic chemistry from The Ohio State University, Columbus, in 1995.

He was a Postdoctoral Fellow in the group of Prof. G. Whitesides in the Department of Chemistry and Chemical Biology, Harvard University, from 1995 to 1998. He is a Cofounder and Senior Scientist at Surface Logix, Brighton, MA. His expertise is in surface chemistry, microfabrication by soft lithography, and materials science.

Anthony G. Evans received the Ph.D. degree in metallurgy at Imperial College, London University, U.K., in 1967.

Since then, he has worked at Rockwell International; the National Bureau of Standards; the University of California, Berkeley and Santa Barbara; and Harvard University. He joined the Faculty of Princeton University, Princeton, NJ, in 1998, where he is now Director of the Princeton Materials Institute and Gordon Wu Professor of Mechanical and Aerospace Engineering. His research has been on the properties and performance of thermostructural materials and systems, such as metals, ceramics, composites, multilayers, and cellular solids for application in aerospace, automotive, power generation, and electronics industries.

George M. Whitesides (M'89) was born in 1939, in Louisville, KY. He received the A.B. degree from Harvard University, Cambridge, MA, in 1960 and the Ph.D. degree from the California Institute of Technology, Pasadena, in 1964.

He was a Member of the Faculty of the Massachusetts Institute of Technology, Cambridge, from 1963 to 1982. He joined the Department of Chemistry, Harvard University, Cambridge, MA, in 1982 and was Department Chairman from 1986 to 1989. He is now Mallinckrodt Professor of Chemistry at Harvard University. His present research interests include materials science, biophysics, surface science, polyvalency, microfluidics, optics, self-assembly, microfabrication, nanotechnology, and cell surface biochemistry.